DIVISION OF COMPUTATIONAL PHYSICS ANNUAL MEETING:
Conference on Computational Physics 2002
25–28 August 2002, San Diego

The First Half Century of the Particle-in–Cell Method

J. U. Brackbill
LOS ALAMOS NATIONAL LABORATORY

26 August 2002

Dedication

To Frank Harlow for his pioneering work in computational fluid dynamics, including the invention of the Particle-in-Cell (PIC), Marker-in-Cell (MAC), Incompressible Eulerian (ICE) and turbulence transport methods, his many popular articles on scientific computing, and his half-century of service to Los Alamos.

Acknowledgements

Contributions from Scott Bardenhagen, Deborah Sulsky, Giovanni Lapenta, and Paolo Ricci to the work presented here are gratefully acknowledged.

Particle-in-Cell

- two meshes ... Eulerian and Lagrangian
  - Eulerian mesh is fixed in space
    - scratch pad for dynamics
    - stores velocity, internal energy and mass
  - Lagrangian mesh moves with fluid
    - Lagrangian mesh is distributed point set of particles
    - fluid motion modeled by particle motion

- two phases, Lagrangian and Eulerian
  - Lagrangian phase: solve equations of motion on grid as though it were a Lagrangian grid
    * grid and particles move together
    * particles move to final position
  - Eulerian phase: restore Eulerian grid
    * particles stationary, but cell boundaries pass over particles
    * mass, momentum and energy repartitioned among cells in proportion to the mass carried by particles from cell to cell

Clouds-In-Cells

PIC for plasma simulation

- particle p assigned position $\mathbf{x}_p$, velocity $\mathbf{v}_p$, mass m_p, and charge q_p
  - initial particle velocity taken from single particle distribution
- charge density $\rho(\mathbf{x})$, computed on a grid by area weighting

$$\rho(\mathbf{x}) = \sum_p q_p S(\mathbf{x} - \mathbf{x}_p; h) \tag{1}$$

- electric field, $\mathbf{E}$, computed on grid

$$\nabla \cdot \mathbf{E} = -\rho \tag{2}$$

- electric field interpolated from grid to particle using area-weighting

$$\mathbf{E}(\mathbf{x}_p) = \sum_g \mathbf{E}_g S(\mathbf{x} - \mathbf{x}_p) \tag{3}$$

- solve particle equations of motion

$$m_p \frac{d\mathbf{u}_p}{dt} = q_p \mathbf{E}(\mathbf{x}_p) \tag{4}$$

$$\frac{d\mathbf{x}_p}{dt} = \mathbf{u}_p \tag{5}$$

ref: Birdsall and Fuss, "Clouds-in-clouds, clouds-in-cells physics for many-body plasma simulation", J. Comput. Phys. **3**, 494 (1969).

FLuid Implicit PIC

- introduces aspects of kinetic simuations into fluid modeling
  - particle velocity, $\mathbf{v}_p$, persistent
  - velocity updated by forces interpolated from the grid, but not replaced

$$m_p \frac{d\mathbf{v}_p}{dt} = \sum_g \mathbf{F}_g S(\mathbf{x} - \mathbf{x}_g) \tag{6}$$

- but retains key feature of Harlow's PIC
  - particles move with area-weighted grid velocity

$$\frac{d\mathbf{x}_p}{dt} = \sum_g \mathbf{v}_g S(\mathbf{x}_p - \mathbf{x}_g) \tag{7}$$

  - grid velocity Fabre average of particle velocities

$$\mathbf{v}_g = \frac{\sum m_p \mathbf{v}_p S(\mathbf{x}_p - \mathbf{x}_g)}{\sum_p m_p S(\mathbf{x}_p - \mathbf{x}_g)} \tag{8}$$

"it may be better to think of the simulation particles as Lagrangian mesh points randomly embedded in a collisionless phase fluid than as fat real particles" Dickman, Morse, and Nielson, "Numerical simulation of axisymmetric, collisionless, finite β plasma", Phys. Fluids, **2**, 1708, 1969.

Perspectives on FLIP

- 1. FLIP is tranlationally and rotationally invariant

- 2-4. Computers are bigger than they were in 1960

- 5. FLIP is an all flow speeds method

Granular Flow

- equations of motion

$$\frac{d\rho_g}{dt} = -\rho_g \nabla \cdot \mathbf{v}_g, \tag{1}$$

$$\frac{d\sigma_g}{dt} = \mathbf{T}_g : \frac{d\mathbf{e}_g}{dt}, \tag{2}$$

$$\frac{d\mathbf{e}_g}{dt} = \frac{1}{2}\left(\nabla \mathbf{v}_g + \nabla \mathbf{v}_g{}^T\right). \tag{3}$$

$$\rho_g \frac{d\mathbf{v}_g}{dt} = \nabla \cdot \sigma_g + \sum_{g'} \rho_g \mathbf{f}_{gg'}, \tag{4}$$

  - $\mathbf{f}_{gg'}$ is the specific contact force exerted on grain g by grain g'.

Implicit and Explicit MPM

- implicit MPM

$$\mathbf{e}_p^1 - \mathbf{e}_p^0 = \frac{1}{2}\sum_i \left[\nabla_{pi}\mathbf{v}_i^\theta + \nabla_{pi}\mathbf{v}_i^{\theta T}\right]\Delta t, \quad (5)$$

$$V_p^1 - V_p^0 = -V_p^0 \sum_i \left[\nabla_{pi}\cdot\mathbf{v}_i^\theta\right] \; Deltat, \quad (6)$$

$$\sigma_p^1 - \sigma_p^0 = \mathbf{T} : (\mathbf{e}_p^1 - \mathbf{e}_p^0), \quad (7)$$

$$m_i\frac{\mathbf{v}_i^1 - \mathbf{v}_i^0}{\Delta t} = -\sum_p \nabla_{pi}\cdot\left(\sigma_p^\theta V_p^\theta\right) + m_i\underline{\mathrm{f}}f_i^\theta, \quad (8)$$

  - $\mathbf{f}_i$ is the value of the specific force of constraint
  - $\frac{1}{2} \leq \theta \leq 1.$

- explicit MPM (leapfrog)

$$V_p^{1/2} - V_p^{-1/2} = -V_p^{-1/2} \sum_i \left[\nabla_{pi} \cdot \mathbf{v}_i^0 \right] \Delta t. \tag{9}$$

$$\sigma^{1/2} - \sigma^{-1/2} = \mathbf{T} : (\mathbf{e}^{1/2} - \mathbf{e}^{-1/2}), \tag{10}$$

$$\mathbf{e}^{1/2} - \mathbf{e}^{-1/2} = \frac{1}{2} \left(\nabla \mathbf{v}^0 + \nabla \mathbf{v}^{0T} \right) \Delta t. \tag{11}$$

$$m_i \frac{\mathbf{v}_i^1 - \mathbf{v}_i^0}{\Delta t} = -\sum_p \nabla_{pi} \cdot \left(\sigma_p^{1/2} V_p^{1/2} \right) + m_i \mathbf{f}_i^0. \tag{12}$$

Nonlinear Stability

- implicit solutions bounded in L_2 norm

$$E^n = E^{n-1}$$

$$-(\theta - \tfrac{1}{2}) \sum_p \left[m_p (\mathbf{v}_p^n - \mathbf{v}_p^{n-1})^2 \right]$$

$$-(\theta - \tfrac{1}{2}) \sum_p \left[(\mathbf{e}_p^n - \mathbf{e}_p^{n-1}) : \mathbf{T} : (\mathbf{e}_p^n - \mathbf{e}_p^{n-1}) \right]$$

(13)

- explicit solutions are not bounded

$$E^n = \frac{1}{2} \left[m(\mathbf{v}^n)^2 + \mathcal{K} \mathbf{x}^{n-\frac{1}{2}} \cdot \mathbf{x}^{n+\frac{1}{2}} \right], \quad (14)$$

or

$$E^{n+\frac{1}{2}} = \frac{1}{2} \left[m \mathbf{v}^n \cdot \mathbf{v}^{n+1} + \mathcal{K} \mathbf{x}^{n+\frac{1}{2}} \cdot \mathbf{x}^{n+\frac{1}{2}} \right]. \quad (15)$$

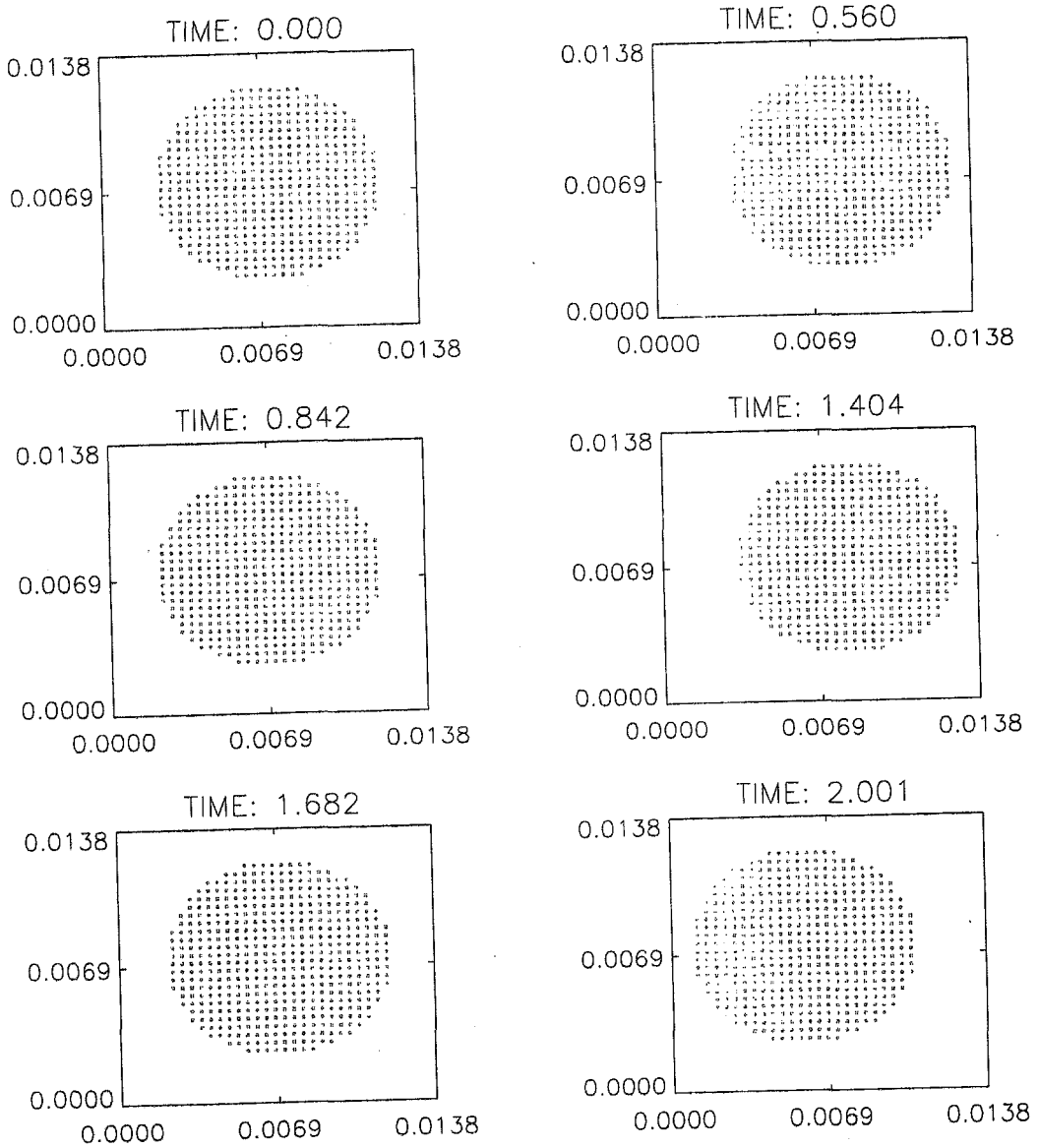

Figure 1: Grain positions in the elastic rebounding grain problem using the implicit MPM formulation.

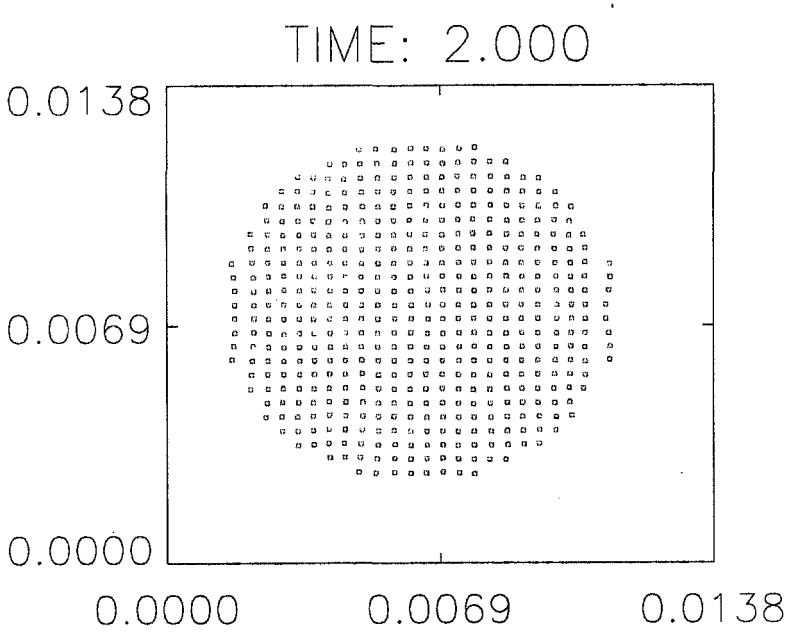

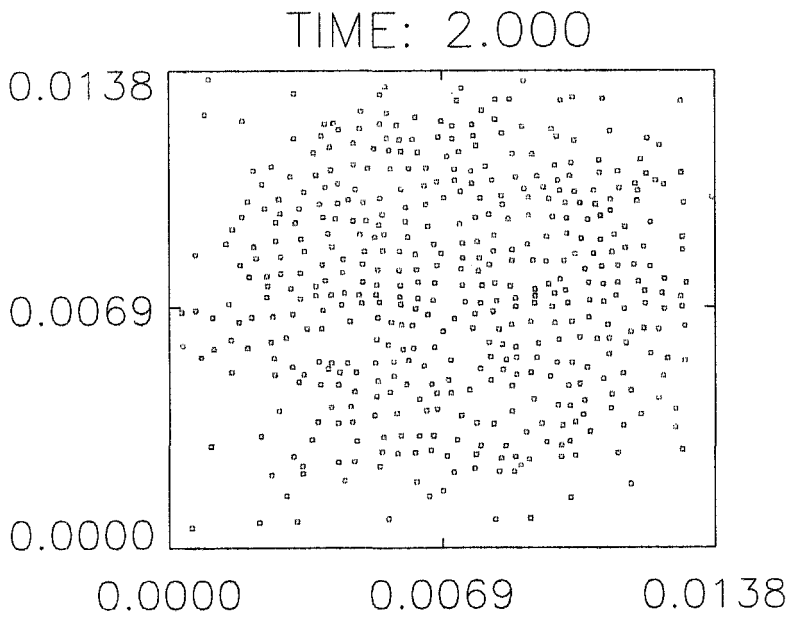

Figure 2: Grain positions at time $t = 2.00$ in the elastic rebounding grain problem using the explicit MPM formulation with a CFL stability limit of $\alpha = 0.25$ and $\alpha = 1.00$.

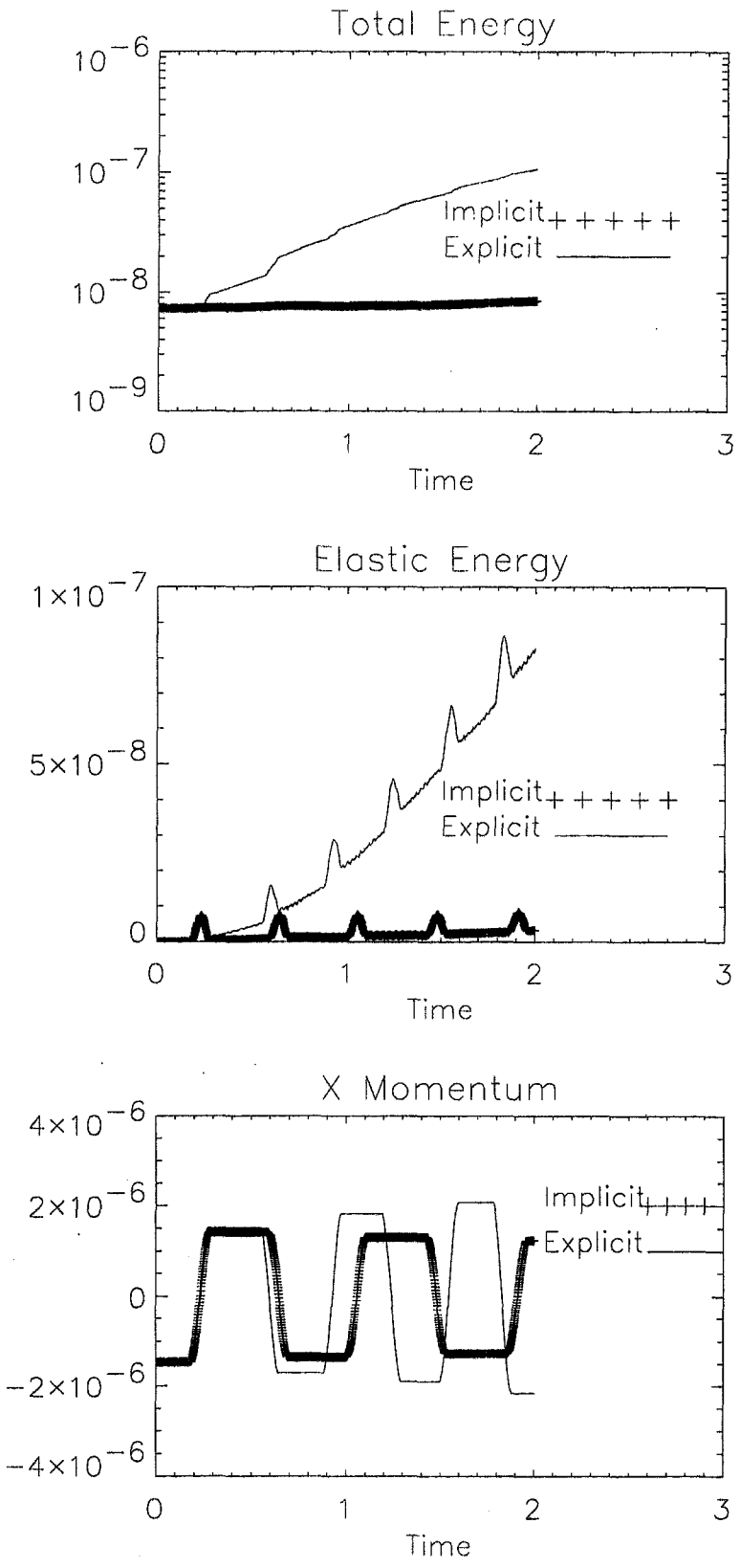

Figure 3: Total energy, elastic energy and x-momentum comparisons for the implicit and explicit formulations for the rebounding elastic grain problem.

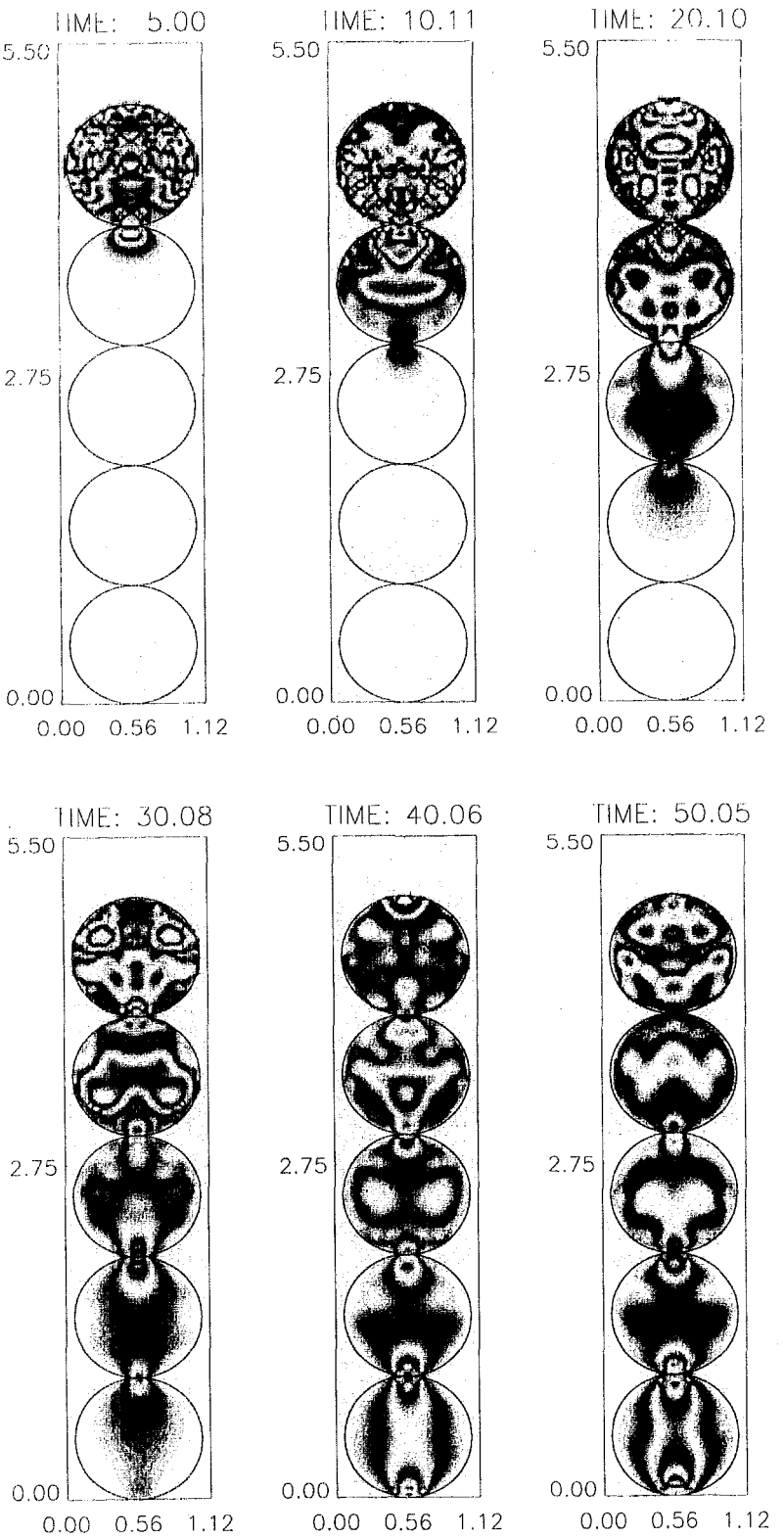

Figure 4: Fringe plots of the principle stress differences for the compressed grain problem using the implicit MPM formulation.

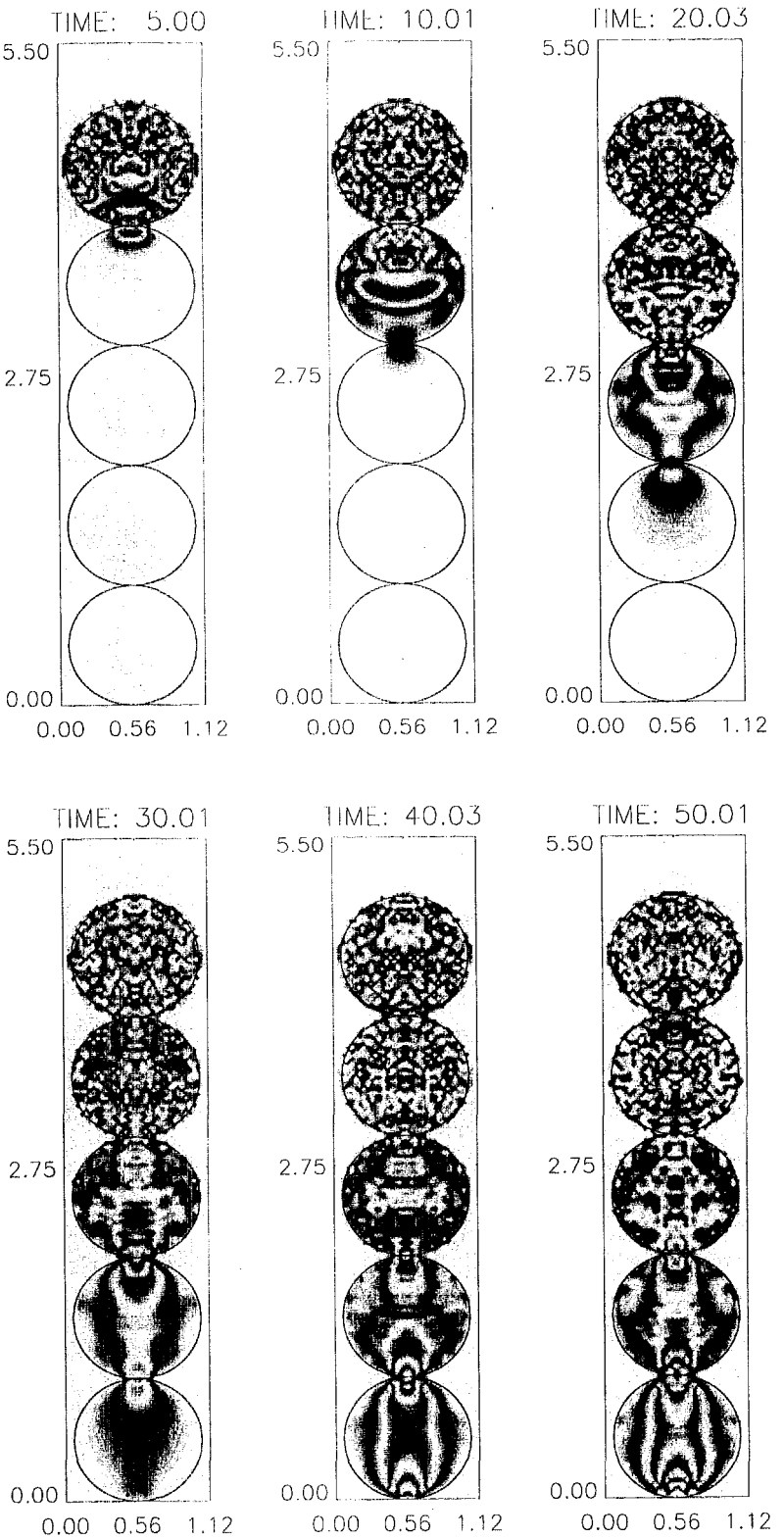

Figure 5: Fringe plots of the principle stress differences for the compressed grain problem using the explicit MPM formulation. The CFL stability limit is $\alpha = 0.25$.

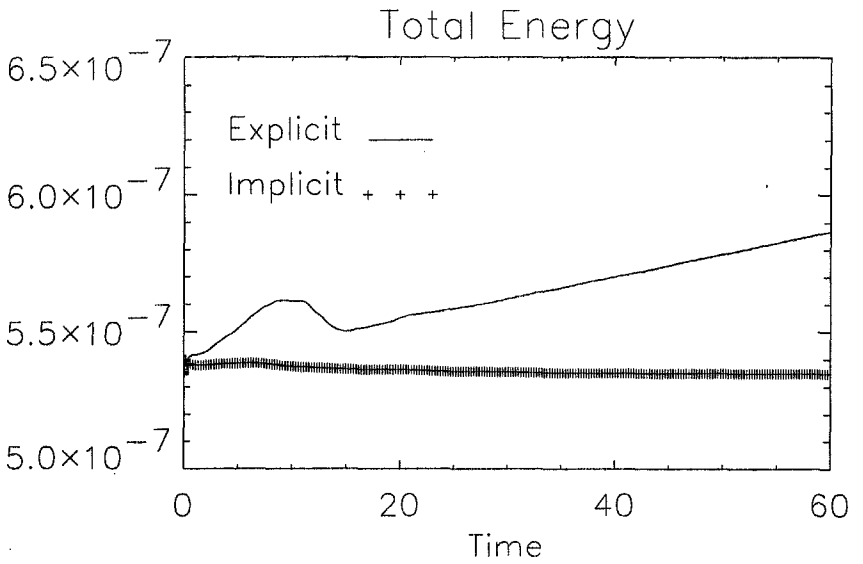

Figure 6: Total energy comparisons for the compressed grain simulation for the implicit and explicit MPM formulation.

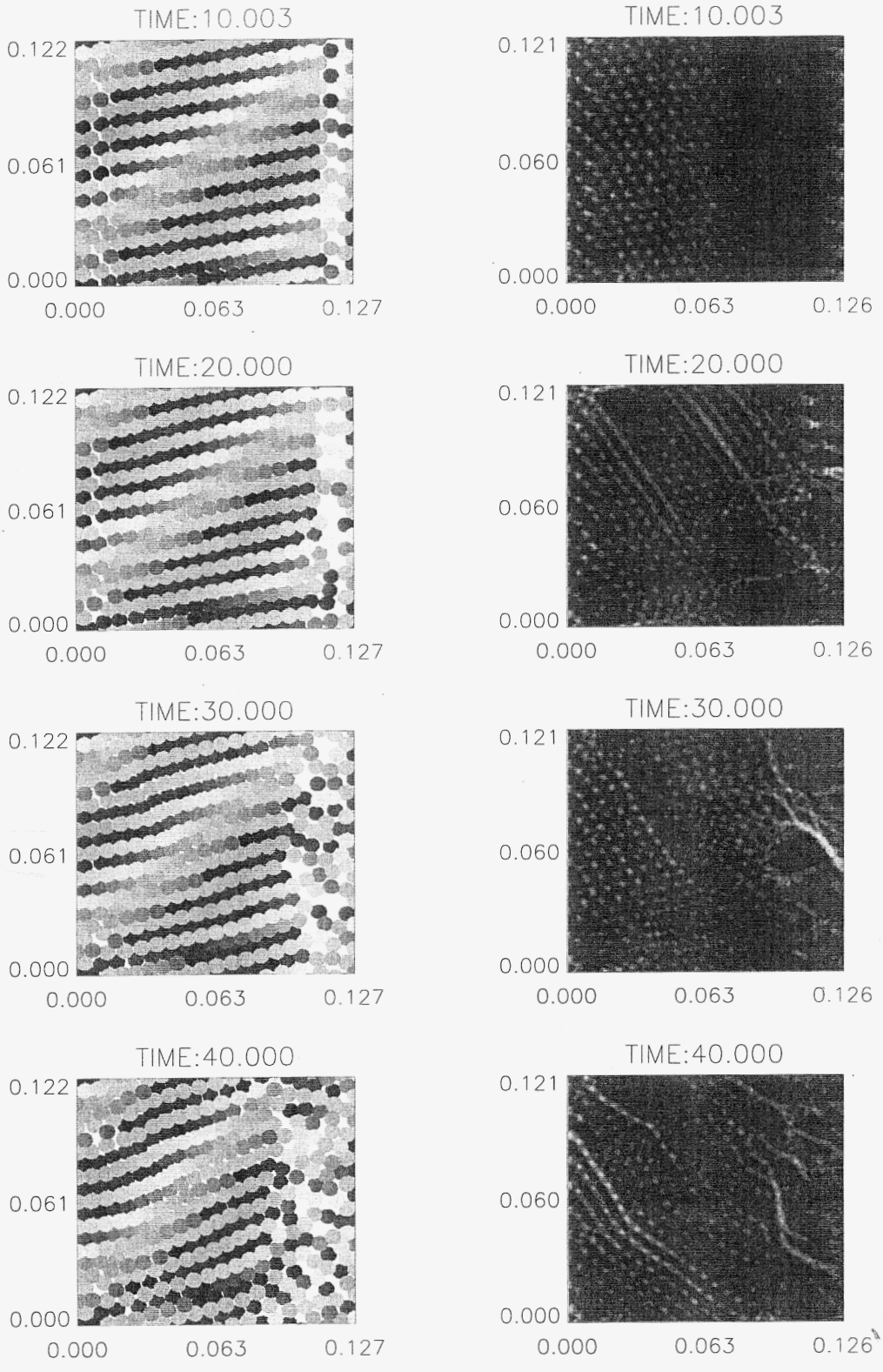

Figure 7: Particle positions and principle stress differences in the monodisperse shearing problem using the implicit MPM formulation.

Implicit Moment Method

- combines fluid PIC with kinetic simulations
  - moment definitions

$$\begin{aligned}\rho(\mathbf{r}) &= \Sigma_p\, q_p S^{(l)}(\mathbf{r}-\mathbf{r}_p)\\ \mathbf{J}(\mathbf{r}) &= \Sigma_p\, q_p \mathbf{u}_p S^{(l-1)}(\mathbf{r}-\mathbf{r}_p)\\ \mathbf{P}(\mathbf{r}) &= \Sigma_p\, m_p \mathbf{u}_p \mathbf{u}_p S^{(l-2)}(\mathbf{r}-\mathbf{r}_p)\end{aligned} \tag{9}$$

  - Maxwell's equations

$$\begin{cases}\nabla\times\mathbf{E}^{n+\theta}+\dfrac{1}{c}\dfrac{\mathbf{B}^{n+1}-\mathbf{B}^{n}}{\Delta t}=0\\ \nabla\times\mathbf{B}^{n+\theta}-\dfrac{1}{c}\dfrac{\mathbf{E}^{n+1}-\mathbf{E}^{n}}{\Delta t}=\dfrac{4\pi}{c}\mathbf{J}^{n+\frac{1}{2}}\\ \nabla\cdot\mathbf{E}^{n+\theta}=4\pi\rho^{n+\theta}\\ \nabla\cdot\mathbf{B}^{n}=\nabla\cdot\mathbf{B}^{n+1}=0,\end{cases} \tag{10}$$

  - fluid equations

$$\frac{\rho^{n+1}-\rho^{n}}{\Delta t}+\nabla\cdot\mathbf{J}^{n+\frac{1}{2}}=0, \tag{11}$$

  and

$$\frac{\mathbf{J}^{n+1}-\mathbf{J}^{n}}{\Delta t}=\frac{q}{m}\left[\rho^{n}\mathbf{E}^{n+\theta}+\frac{\mathbf{J}^{n+\frac{1}{2}}\times\mathbf{B}^{n}}{c}-\nabla\cdot\mathbf{P}^{n}\right], \tag{12}$$

  - closure assumption

$$\frac{\mathbf{v}_{thermal}\Delta t}{\Delta x}<1 \tag{13}$$

- possible to model low-frequency modes with realistic mass ratios
- scaling of relative cost of explicit and implicit simulations

$$cost\frac{explicit}{implicit}\approx\frac{m_i}{m_e}^{\frac{d+1}{2}}$$

Cost Comparison: Explicit and Implicit Simulations

- $m_i/m_e = 25$
- CELESTE3D (implicit)
  - $N_x \times N_y = 64 \times 64$
  - $2 \cdot 10^5 particles$
  - $\omega_{pe}\Delta t = 1.5$
- explicit simulation
  - $N_x \times N_y = 512 \times 256$
  - $9.12 \cdot 10^6 particles$
  - $\omega_{pe}\Delta t = 0.15$

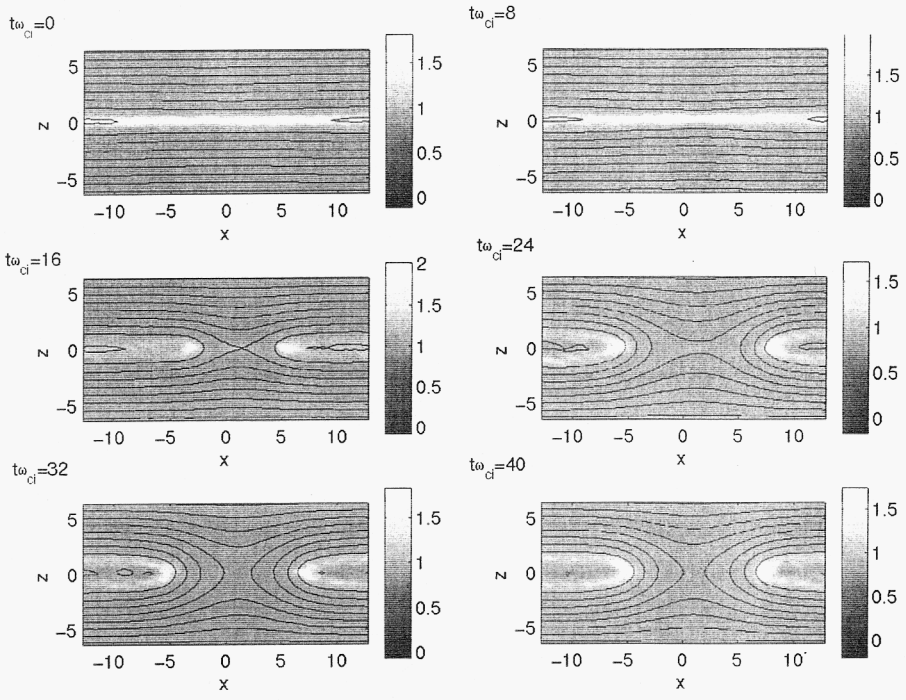

Figure 8: Evolution of the magnetic field and evolution of the out-of-plane current density (color coded) for the simulation whose parameters match those ones of the GEM hallenge. This figure is in agreement with Plate 1 in Ref. [?].

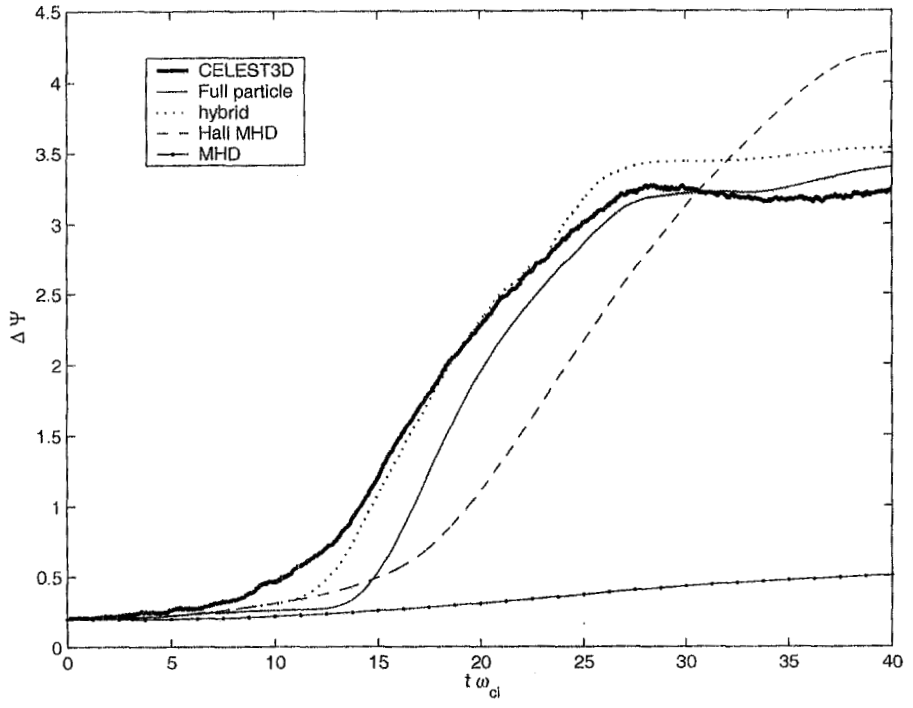

Figure 9: Reconnected flux, $\Delta\Psi$, as a function of time, for the GEM magnetic reconnection challenge [?]. The reconnection rate reported by CELESTE3D is compared with the results (provided by J.F. Drake and M.A. Shay) of the different codes which have performed the GEM challenge (see Fig. 1 of Ref. [?]).

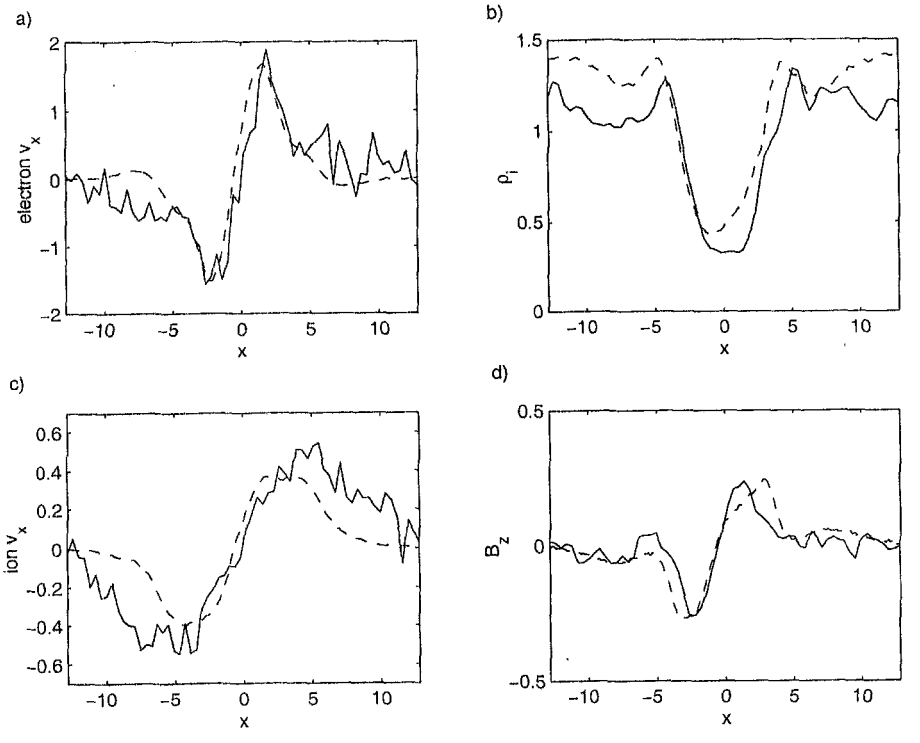

Figure 10: Comparison between CELESTE3D (solid line) and the explicit kinetic simulation data provided by P.L. Pritchett (see Ref. [?], Figs. 4,6) (dashed line) of the x-component of the electron velocity (a), ion density (b), x-component of the ion velocity (c) and z-component of the magnetic field (d), as a function of x and at $z = 0$, when $\Delta\Psi = 1$ [averaged between $t\omega_{ci} = 15$ and $t\omega_{ci} = 15.6$ (a-c) and at $t\omega_{ci} = 15$ (d) for Pritchett's simulation] within the GEM magnetic reconnection challenge. The results reported in this figure can also be compared with Fig. 9 of Ref. [?].

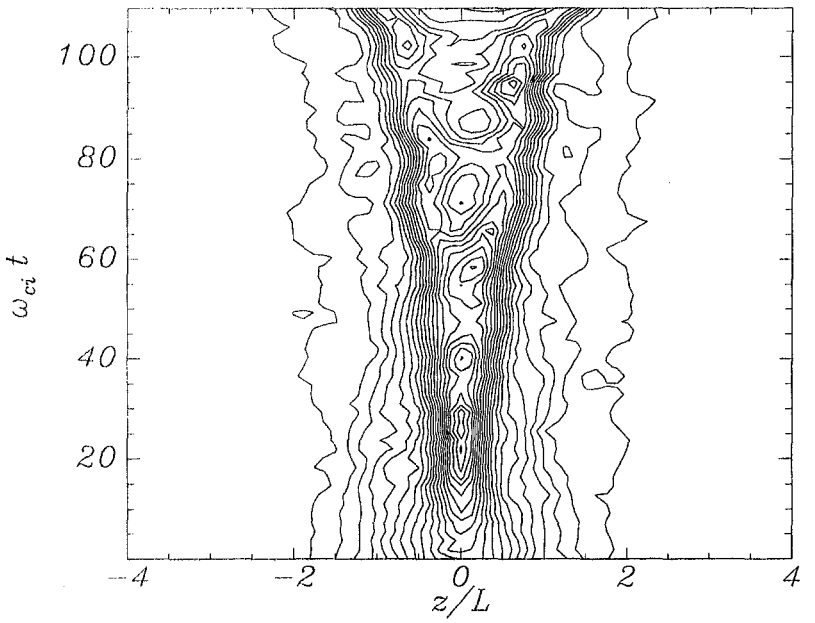

Figure 11: Time evolution of $J_y(z)$ (averaged in the y direction). The case considered has $m_i/m_e = 180$, $u_i/v_{th,i} = 1$ and $T_i/T_e = 1$

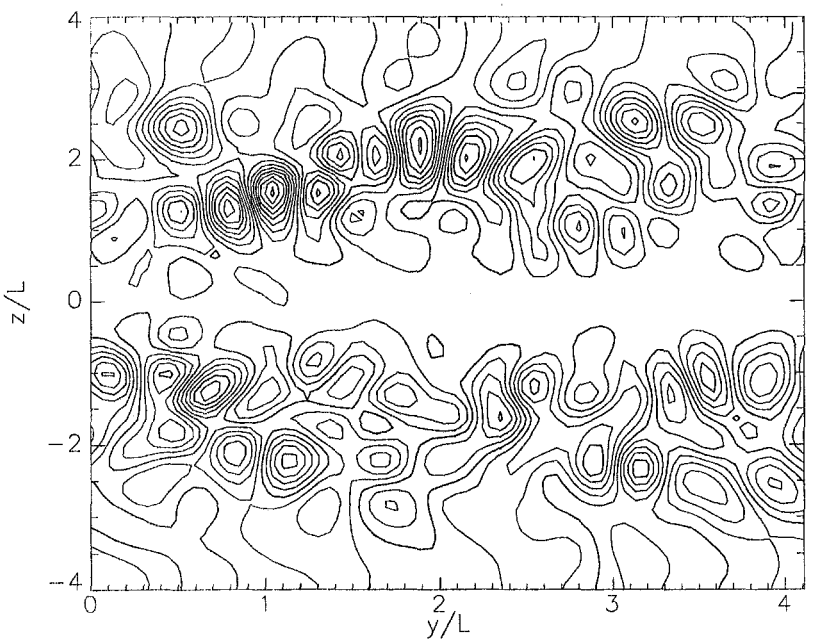

Figure 12: Contour plot of E_y at $\omega_{ci}t = 7$ with $u_i/v_i = 1$, $T_i/T_e = 4$, $m_i/m_e = 180$, $L_y/L = 4$. Note that the dominant LHDI mode has $m_y = 8$, corresponding to $k_y L = 12.5$.

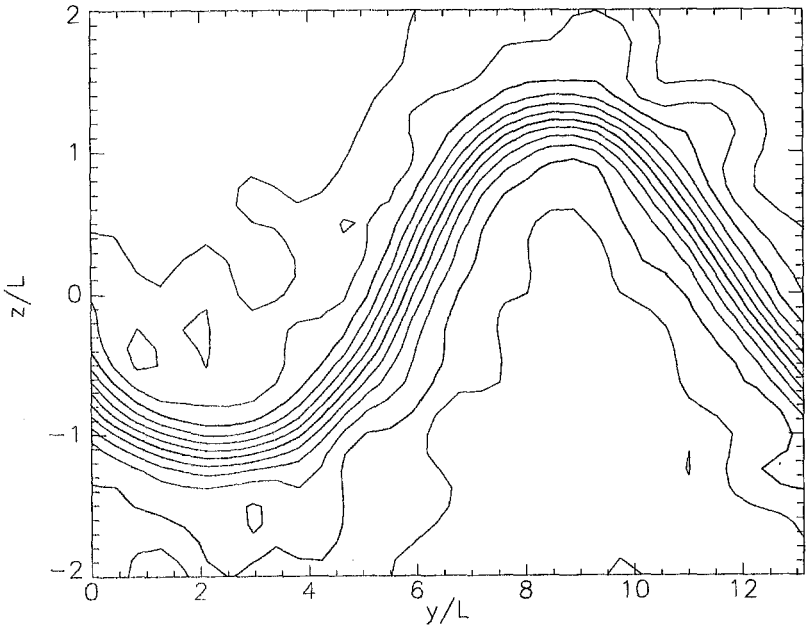

Figure 13: Contour plot of $B_x(y,z)$ at the end of the simulation ($\omega_{ci}t = 110$). The case considered has $m_i/m_e = 180$, $u_i/v_{th,i} = 1$ and $T_i/T_e = 2$. Note that only a portion of the system, $-2 \leq z/L \leq 2$, is shown (the total vertical size is $L_y/L = 9$).

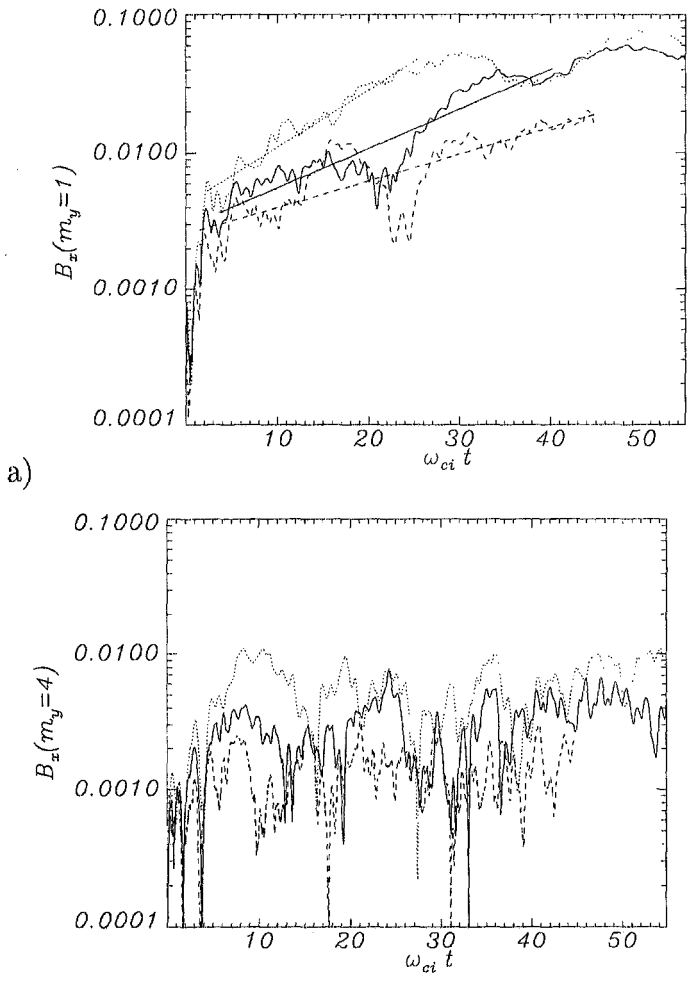

Figure 14: Evolution of the KM (a) and of the LHDI (b), for a current sheet with $u_i/v_i = 1$. Three runs are shown, with different temperatures: $T_i/T_e = 1$ (dashed); $T_i/T_e = 2$ (solid); $T_i/T_e = 4$ (dotted). A best fit of the second phase of the evolution (shown with the straight lines in figure) gives the following growth rates: $\gamma/\omega_{ci} = 0.1, 0.07$, and 0.04 for $T_i/T_e = 4, 2$, and 1 repectively. The saturation level of the LHDI is computed as the L_2 norm of the Fourier component shown in plate (b) integrated in time between $\omega_{ci}t = 10$ and the end of the simulation: $< B_x(m_y = 4)^2 >^{1/2} = 6.5 \cdot 10^{-3}$, $3.5 \cdot 10^{-3}$, and $1.5 \cdot 10^{-3}$ for $T_i/T_e = 4, 2$, and 1.

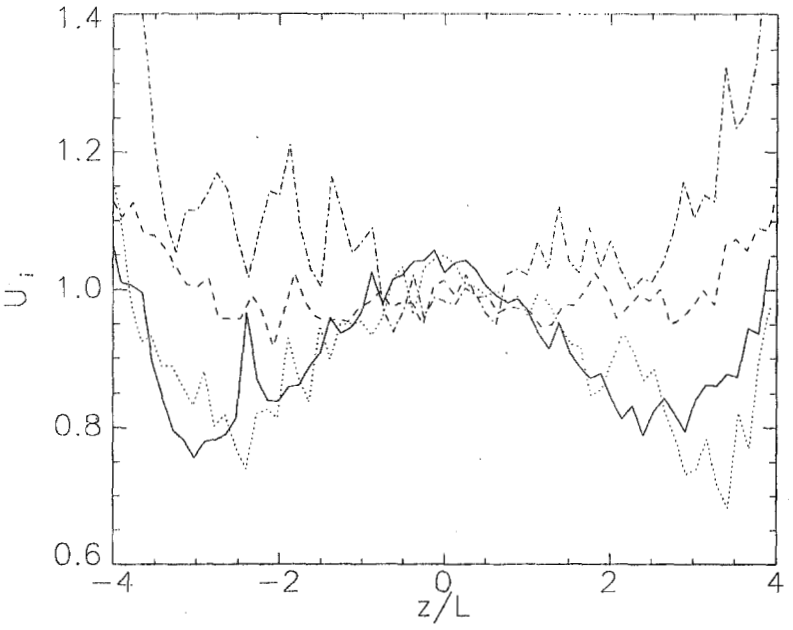

Figure 15: Velocity profile at time $\omega_{ci}t = 12$ for a system with $u_i/v_i = 1$, $m_i/m_e = 180$ and with four different temperature ratios: $T_i/T_e = 10$ (solid); $T_i/T_e = 4$ (dotted); $T_i/T_e = 2$ (dashed); $T_i/T_e = 1$ (dash-dotted)

Concluding Remarks

- haven't mentioned many other developments
  - magnetohydrodynamics
  - suspension flow
  - particle rezoning
- current work
  - multiscale problems
  - quantum mechanics?

Session F1 - Something Old and Something New.
INVITED session, Tuesday morning, August 27
Regency Ballroom, Hyatt Regency Islandia

[F1.001] The First Half Century of the Particle-in-Cell Method

J. U. Brackbill (Theoretical Division, Los Alamos National Laboratory)

While this talk is mainly about new results for magnetic reconnection, we will discuss the state of Harlow's particle-in-cell method (PIC) after its first half century. PIC is a remarkably versatile method. It was the first method to model high-speed and free-surface flow in two dimensions, and the first to model collisionless plasmas in two space dimensions. The versatility can be explained by PIC's use of Lagrangian and Eulerian descriptions in a complementary way, which, for example, allows one to model granular material in all its complexity, including history-dependent material response, Coulomb friction, and bonding. Recently, an implicit granular flow method confimed an old conjecture about the connection beween the finite grid instability, nonlinear stability, and energy conservation in PIC plasma simulation. New techniques, including Newton Krylov solvers for the field equations and a new understanding of the correct boundary conditions, result in accurate and robust implicit plasma simulations with the ability to simulate more realistic electron-ion mass ratios. Results from magnetic reconnection studies illustrate why this is important, the role of the lower-hybrid drift instability in symmetry breaking, and magnetic reconnection in the magnetotail, even with a perpendicular field.

[F1.002] Cluster Analysis of DNA-chip data

Eytan Domany (Dept. of Physics of Complex Systems, Weizmann Inst. of Science, Rehovot 76100 ISRAEL)

DNA chips are novel experimental tools that have revolutionized research in molecular biology and generated considerable excitement. A single chip allows simultaneous measurement of the level at which thousands of genes are expressed. A typical experiment uses a few tens of such chips, each focusing on one sample - such as material extracted from particular tumor. Hence the results of such an experiment contain several hundred thousand numbers, that come in the form of a table, of several thousand rows (one for each gene) and 50 - 100 columns (one for each sample). We developed a clustering methodology to mine such data.

This talk will provide a very basic introduction, with no prior knowledge of any biology assumed. I will explain what genes are, what is gene expression and how it is measured by DNA chips. I will also explain what is meant by "clustering" and how we analyze the massive amounts of data from such experiments, using a novel method called Coupled Two Way Clustering [1], and present results obtained from analysis of several types of cancer. If time permits, I will mention briefly how similar methods can be applied to other problem areas, such as document classification, antigen chips and the low-temperature phases of short range spin glasses.

[1] G. Getz, E. Levine, and E. Domany, PNAS 97, 12079 (2000)